Two-Scale Methods for LES / URANS

L. He
University of Oxford
Department of Engineering Science
Oxford, OX2 0ES
United Kingdom

Abstract

A common challenge in CFD simulations for both external and internal flows is in the near-wall region for wall-bounded turbulent flows. Fully wall-resolved LES (WRLES) solutions tend to be very costly particularly at realistically high Reynolds numbers, whilst wall-modeled LES (WMLES) are subject to considerable empiricism, further challenged by more recent findings on how outer flow large-scale coherent structures may influence inner near-wall flow small scales. The two-scale LES development is aimed at being much more affordable than WRLES and much less empirical than WMLES.

It must be noted that the cost benefit of WMLES by using a coarse mesh in the near wall region will inevitably be tied to its own price in under-resolution associated numerical errors. The very mesh-dependent nature of the errors means that an effective correction needs to be 'mesh-informed', and preferably can be enacted in-situ in a solution process. The two-scale framework is formulated to provide such correction: coupling between a local fine-mesh block (or a small number of local fine-mesh blocks) and a global coarse-mesh domain. This is achieved by harnessing the source terms arising from the imbalance when a finely resolved solution is projected to a coarse discrete space (under-resolved mesh), akin to the nonlinear product terms ('Reynolds stresses') in time-averaging flow equations. A space-time averaging is purposely introduced in either a direct or an inverse mode in the global domain and the local block respectively. The source terms in a compact form (one scalar for one flow equation) are directly obtained by simply taking the coarse-mesh residual using the space-time averaged fine-mesh solution. These 'mesh-informed' source terms updated on-the-fly enable mutual interactions between the local and global domain during a solution process. The converged solution for this two-scale coupled system should meet two seemingly conflicting requirements: an otherwise poorly conditioned local fine-mesh block is now subject to adequate environment/flow condition, and an otherwise poorly resolved global coarse-mesh domain is now effectively subject to high resolution.

In this lecture, the primary motivating considerations, the framework approach and the implementation methods will be presented and discussed. The validity and feasibility of the two-scale approach for efficient and accurate scale-resolving turbulent flow simulations will be illustrated in a range of cases of fundamental as well as practical interest.

1. Introduction: Established vs Emerging Consensus on Wall-bound Turbulence

The two-scale approach to wall-bound turbulent flows has been developed in the past 15 years or so, initially for RANS/URANS (e.g. He 2013 [1]), more recently for LES (He 2018 [2], Chen and He 2022 [3]). Given the context of the lecture series, we will mainly focus on LES in this lecture.

For high-fidelity turbulence scale-resolving computational method development and applications, a topic of general interest is how to deal with the near-wall region efficiently and accurately. We will first take a brief look at the classic view on near-wall flow physical characteristics and related computational simulation/modelling development. Then some new observations and emerging consensus based on more recent experimental measurements, high-fidelity simulations and data-processing techniques will be discussed. The implications for the near-wall flow modelling also serve as a further motivating consideration for the two-scale LES development.

1.1. Near-wall Region: Focal Point for Turbulence Resolving/Modelling Approaches

The challenges in scale-resolving computations of wall bound turbulent flows arise from a wide range of temporal and spatial length scales involved, particularly at high Reynolds numbers. Consequently, DNS to resolve all turbulence scales tend to be prohibitively expensive. The computational cost for DNS in terms of mesh count roughly scales with Reynolds number as $O(Re^3)$ (e.g. Jimenez 2003 [4]). LES solutions filtering out small scales to be modelled are a less costly alternative with clear and consistent modelling fidelity generally. Nevertheless, the mesh count required for LES still scales with Re as $O(Re^2)$ (Mizuno & Jiménez 2013 [5]). Thus the cost of full LES computations is still far too expensive for many practical engineering applications.

The near wall region is where the turbulence activities are most intensive, not only in terms of the level of turbulence but also the dynamics affecting the overall time-mean flow performance. This is also where the required mesh resolution is the highest due to the very small spatial and temporal scales of turbulence fluctuations.

A long-held consensus is that all near wall turbulence behaves similarly in a self-sustained manner. The seemingly 'universal' autonomous behaviour provides a strong impetus to develop a modelled, instead of resolved, treatment for the near wall turbulent flow region. This provides a strong motivation for the development of a hybrid approach with a scale-resolving outer flow region coupled with a modelled (typically with a Reynolds Averaged Navier-Stokes, RANS model) inner near-wall region, notably by Spalart et al 1997 [6], Spalart 2009 [7]. The wall-modelled LES (WMLES) may be justified based on the universality of 'autonomous' self-sustained small scale turbulence dynamics in the near-wall region. Thus. it seems reasonable that the small scales in the near-wall 'inner' region and the large coherent scales in the log-law governed 'outer' region can be treated completely differently. The assumption of 'scale-separation' between those scales in the outer and inner regions would seemingly justify the WMLES approach: resolving the large-scales in the outer region, while modelling the more 'universally' behaving small scales in the near-wall inner region.

The wall-modelled LES makes scale-resolving turbulent flow solutions feasible in large scale complex whilst practically relevant settings, thus has been very appealing. As expected, the accuracy and

applicability of WMLES would have to be affected by the empirical nature of the near-wall RANS modelling, as well as by how the scale-resolving outer flow region is transitioned (also empirically) to a modelled near-wall region. We may wonder, are there any more fundamental challenges to WMLES?

1.2. Recent Findings: New Consensus and Implications

In the past 15 years or so, there has been a significant progress in fundamental understanding of wall-bound turbulent flows at high Reynolds numbers, through both advanced experimental measurements and high-resolution DNS analyses. An emerging new consensus as a result recognises that the near-wall turbulence behaves distinctively with some interesting 'dual' characteristics. In addition to the well-recognised self-sustained 'universal' behaviour and dynamics, near-wall turbulence is shown to be also Reynold number dependent, influenced by large-scale coherent structures in the outer flow region. This observed near-wall flow behaviour does seem to suggest that the previously established and long-held wisdom can only serve as a partial description.

An important aspect of the new findings is the 'foot-printing' on the near wall turbulence by the large coherent structures resident in the log-law region. The velocity field below the buffer region exhibits clear signatures of long streaky outflow structures, as revealed in experiment data (Hutchins & Marusic 2007 [8] ; Marusic et al. 2010 [9]) and DNS results (e.g. Jimenez 2013 [10], Lee & Moser 2015 [11]). Additionally, the near wall turbulence is shown to be subject to interactions between local small scales and those large 'footprints', through a 'modulation' (Mathis et al. 2009 [12]). In a simple term, nonlinear interactions in flow disturbances containing a large scale at frequency ω_L and a small scale at ω_S can generate other scales at frequencies $(\omega_L + \omega_S)$, $(\omega_L - \omega_S)$, $2\omega_L$, $2\omega_S$.

These recent findings on near-wall turbulence have certainly provided extra challenges to existing modelling approaches and underlying wisdoms generally. Various new wall-modelling efforts are made recognising the distinctive scale dependent behaviour as observed, by generating a synthetic boundary condition to mimic the wall effect (Mizuno & Jiménez 2013[5]), or super-imposing the traditional 'universally self-sustained' part and the Re-dependent passively influenced part (Marusic, et al. 2010 [9]; Agostini & Leschziner 2016 [13].

In the context of WMLES, the presence of the outer large scale 'foot-printing' and associated 'modulation' does seem to contradict somewhat the 'scale-separated' treatment for the outer and inner regions. Consequently, it can be argued that the recent findings on the near-wall turbulence behavior have also changed the relative merits of WMLES and WRLES. The increased modelling uncertainties in WMLES will have to be weighed accordingly against the increased cost of WRLES, particularly in more practically relevant high Reynolds number settings.

1.3. Validation and Application Settings for Two-scale Method

The above background in the context of WRLES versus WMLES in general for wall-bound turbulence provides a strong motivation for developing a method which can capture and resolve near-wall small scales under the influence of outer large scales, and do so more efficiently than costly WRLES. The primary intent is to explore the feasibility of leveraging a high-resolution solution in a small local fine-

mesh block (or a small set of such fine-mesh blocks) in near-wall region. The corresponding setup is indicated in Fig.1 for a canonical channel flow where the turbulence statistics remain invariant in the two wall-parallel directions. Fig. 2 shows the setup for a tripped turbulent boundary layer where the turbulent statistics are evolving in the streamwise direction. If the global coarse-mesh domain is used to capture and resolve the large turbulent scales with strong history effects, the key issue to be addresed is: how would the local fine-mesh block and the global coarse-mesh domain interact?

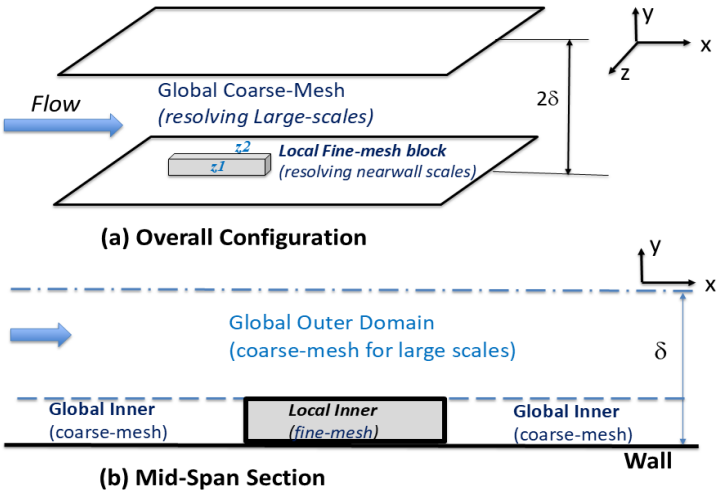

Figure 1: Local Near-wall Fine-mesh Block for Channel Flow.

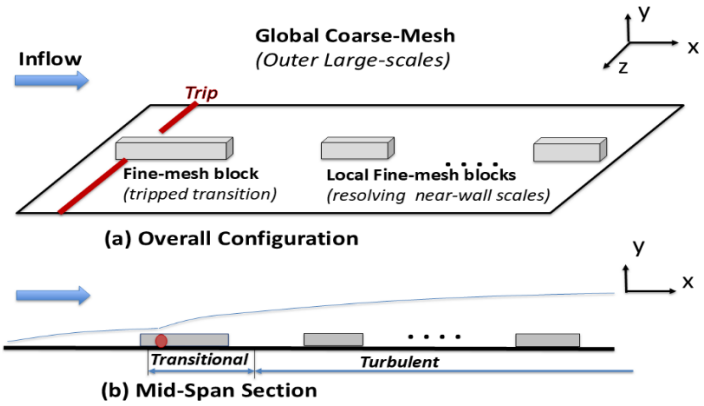

Figure 2: Local Near-wall Fine-mesh Block for Tripped Boundary Layer.

In the context of turbomachinery flows, scale-resolving solutions will have to face the challenge due to the inherent unsteady interactions in a multi-blade passage multi-blade row environment. Consider one single blade-passage domain. A typical mesh count for a RANS is around 1 million whilst its counterpart for a WRLES would be around 100 millions. This rise in computing cost per passage is already very large. A further increase by 1-2 orders of magnitude due to multi-blade passages (30-70 per row) would make it prohibitively expensive. A further question of interest: can we couple a local single-passage fine-mesh block resolving nearwall flow with a global multi-passage coarse-mesh domain capturing and resolving large scales turbulent and other unsteadiness (Fig.3)?

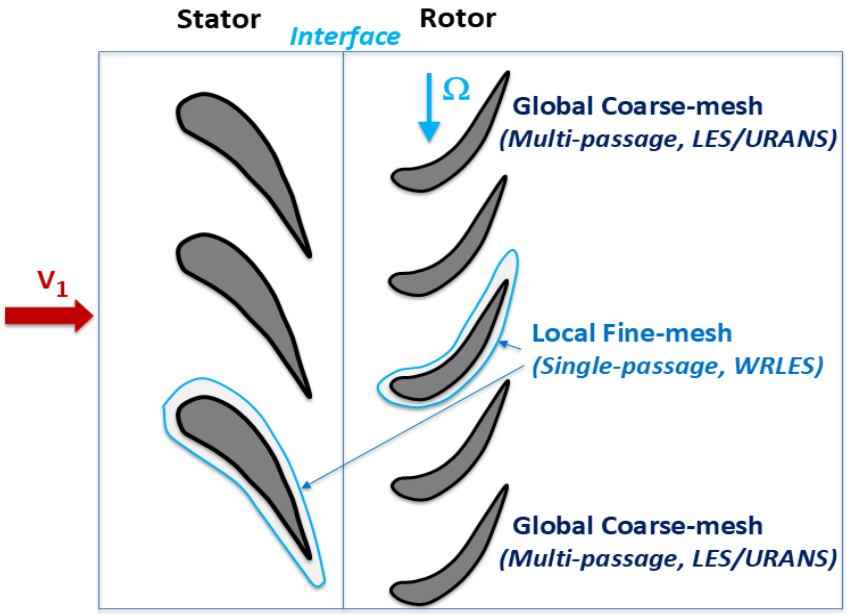

Figure 3: Multiple Blade-rows with Single-passage Fine-mesh Block for Each Row.

2. Two-scale Framework

2.1. Local Resolution vs. Global Condition

We begin by considering two contrasting scenarios of CFD solutions in general:

a) On the one hand, we can easily solve a truncated small domain with a fine mesh and high-fidelity model, but it would be of no use under uncertain environment/boundary conditions.

b) On the other hand, we can easily have well-defined environment/boundary conditions for a large global domain, but the solution would also be of no use if poorly resolved with a coarse mesh.

When we seek a solution of high fidelity as well as high resolution for a large global domain, a direct approach covering all scales will naturally be costly. The basic idea of a two-scale approach is to couple the two 'opposing' parts (the local fine-mesh and the global coarse-mesh domains) to lead to a desired solution. A pathway to take is, on the one hand, to propagate the effect of the local high resolution to the under-resolved coarse-mesh to improve the resolution of the global domain. And on the other hand, the improved global coarse-mesh solution would then in turn improve the conditioning of the local fine-mesh domain. So the starting question is, how should we go about propagating a local solution to a global domain?

Consider a stator-rotor turbine stage. Given a seemingly random instantaneous unsteady turbulent flow (Fig.4a), there does not appear to be any directly definable passage-passage similarity. However, looking at its time-averaged counterpart, we get a very different picture. In fact, for a rotor-stator stage, there is a simple direct passage-passage periodicity (Fig.4b). Also note that the time-averaged flow is spatially much smoother. Thus, even when we deal with unsteady flow with deterministic and non-deterministic disturbances, we shall seek to work through the time-averaged flow.

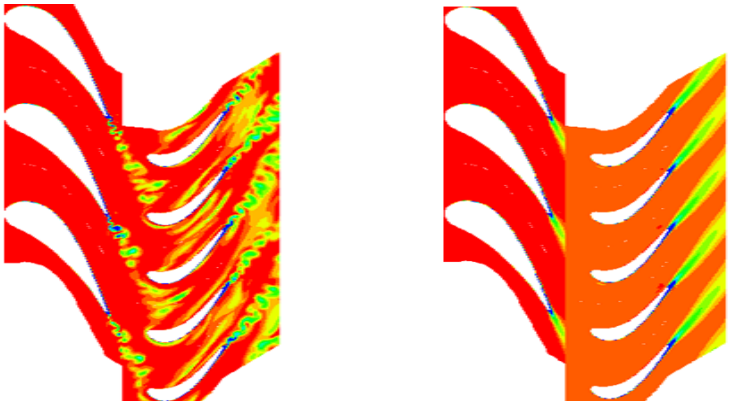

(a) Instantaneous **(b) Time-averaged**

Figure 4: Entropy Contours (*Unsteady vs. Time-averaged*).

We will now consider how to effectively leverage the averaging and propagate the local high-resolution effect to a global domain, to enable the interaction between the two domains and between the two scales for an efficient high-fidelity solution.

2.2. Learning from Reynolds Averaging (Time Averaging)

We now take a slightly different look at the conventional time-averaging in the context of Reynolds-averaging for turbulent flow. Write the full flow equation system in a simple form denoting $\boldsymbol{U}$ as the vector of flow variables:

$$\frac{\partial \boldsymbol{U}}{\partial t} + \boldsymbol{R}(\boldsymbol{U}) = 0 \tag{1}$$

A standard temporal decomposition is given by:

$$\boldsymbol{U}(\boldsymbol{x},\boldsymbol{t}) = \overline{\boldsymbol{U}}(\boldsymbol{x}) + \boldsymbol{U}'(\boldsymbol{x},\boldsymbol{t}) \tag{2}$$

The time-averaging part over a time period T is:

$$\overline{\boldsymbol{U}}(\boldsymbol{x}) = \frac{1}{T}\int_o^T \boldsymbol{U}\boldsymbol{dt}\,, \qquad \overline{\boldsymbol{U}'}(\boldsymbol{x}) = 0$$

Time-averaging the flow equation, we must then have,

$$\overline{\boldsymbol{R}(\boldsymbol{U})} = 0 \tag{3}$$

Due to nonlinearity of the advective fluxes, $\overline{\boldsymbol{R}(\boldsymbol{U})} \neq \boldsymbol{R}(\overline{\boldsymbol{U}})$**,** a well-known consequence of Reynolds averaging. We now purposely express the time-averaged flow equations in two modes. The first one is the common form used for turbulence closure, notionally labeled here as a 'direct mode'.

Reynolds-Averaging ('Direct Mode'): $$\frac{\partial \boldsymbol{U}}{\partial t} + \boldsymbol{R}(\boldsymbol{U}) = \boldsymbol{S_t} \tag{4}$$

$\mathbf{S}_t$ is a vector with three elements for lumped Reynolds stress differential terms (divergence) for momentum, one element for energy, and one zero element for mass continuity. For a compressible flow system, $\mathbf{S_t}$ has 5 scaler elements. For an incompressible flow system, $\mathbf{S_t}$ has 4 scalers as the energy

equation is decoupled from the rest. When the solution to Eq.4 converges to a steady state, it should produce the time-averaged flow field as intended, if correct $\mathbf{S_t}$ can be provided. The direct mode of Reynolds-averaging underlines its basic objective that the time-averaged flow field can now be solved with a much coarse (zero) resolution in time. But in so doing, the otherwise closed flow equation system becomes open. Thus, a correct averaged flow solution with the coarser resolution can only be obtained if the extra nonlinear product terms can be found to balance the equations. The latter has been the motivation of all turbulence modelling developments with a varying extent of empirical ingredients.

It is worth emphasizing that Eq.4 also underlines the general fundamental working for any turbulence models. A turbulence closure can be in all sorts of different forms (e.g. in a simple algebraic mixing-length or extensive differential Reynolds stress terms). But a turbulence model will ultimately affect the flow solution by balancing the flow equations with one scalar source term for each equation respectively, just like one 'body-force' scalar lumping together all differential viscous terms in balancing one momentum equation (Denton 1986 [14]). Basically, in solving the time-averaged flow, the 'direct mode' takes the lumped nonlinear product terms together, one scalar for each equation.

On the other hand, write the time-averaged equation the other way around. We then have the second mode (which has so far been rarely considered).

Reynolds-Averaging ('Inverse Mode'): $\mathbf{S_t} = \mathbf{R}(\bar{\mathbf{U}})$ (5)

Given that one flow equation corresponds to one scalar source, the inverse mode (Eq.5) will explicitly fix the scalar source terms for all the flow equations if the flow field is known. Thus, if we have a given target time-averaged solution ($\bar{\boldsymbol{U}}$) of high fidelity and high resolution (regardless of the origin), we can get those scalar sources (one for each equation) $\mathbf{S_t}$, simply by computing the corresponding flux residuals explicitly and noniteratively using the flow variables of the target solution. As such, these scalar source terms can be used to drive a new solution to reproduce the target (e.g. as shown for vortex-shedding by Ning and He 2001 [15]). This property by itself does not seem to be of any practical use. However, the inverse mode will feature very differently when used in conjunction with the direct mode as part of an interactive procedure of a coupled system, to be introduced next.

2.3. Space-Time Averaging: towards Two-Scale System and Solution

Reynolds-averaging shows how a meaningfully averaged solution of high resolution in time can be obtained through a method with low resolution (or no resolution at all) in time. We now seek to establish a meaningfully averaged flow solution with lower resolution in both space and time.

Consider a two-scale (spatially discrete) system consisting of two mesh domains:

a) *Coarse mesh:* this is for an adequately accurate solution which can be obtained if the scalar sources (similar to the lumped stress terms in Reynolds-averaging) are provided. The corresponding semi-discrete equations with the spatial discretization on the coarse mesh (denoted by subscript 'C') are

$$\frac{\partial \boldsymbol{U_C}}{\partial \boldsymbol{t}} + \boldsymbol{R_C}(\boldsymbol{U_C}) = 0 \qquad (6)$$

where R_C represents the total flux residual discretized on the coarse mesh.

b) <u>*Fine mesh*</u>*:* we build the fine mesh by subdividing the coarse mesh. A coarse mesh cell then consists of a number locally embedded fine-mesh cells. The corresponding semi-discrete form of the equations spatially discretized on the fine-mesh (denoted by subscript 'f') is

$$\frac{\partial \boldsymbol{U_f}}{\partial t} + \boldsymbol{R_f}(\boldsymbol{U_f}) = 0 \tag{7}$$

For a spatial and temporal decomposition, the time-averaging is carried out as usual over the entire time period of the solution. The spatial averaging is carried out *locally* for each coarse mesh cell. Given that the fine-mesh cells are created by simply subdividing a coarse-mesh cell, the local spatial average is defined as a volume-weighted average of flow variables for each coarse-mesh cell. In a discrete form, a flow variable is identified by its corresponding fine-mesh cell index *m*. The instantaneous spatial average for coarse-mesh cell M of total volume V_M at time step *n* becomes,

$$\widetilde{\boldsymbol{U}}(M,n) = \frac{1}{V_M}\sum_{m=1}^{N_m} \boldsymbol{U}(m,n) v_m \tag{8}$$

N_m is the number of fine-mesh cells with volume of v_m, (m=1, …, N_m) contained in coarse-mesh cell M. The corresponding space-time average for coarse-mesh cell M is then,

$$\overline{\widetilde{\boldsymbol{U}}}(M) = \frac{1}{N_t}\sum_{n=1,}^{N_t} \widetilde{\boldsymbol{U}}(M,n) \tag{9}$$

N_t is the total number of time steps with a constant physical time step size being assumed. Note that the space-time averaging is a simple sum of corresponding instantaneous variables in time and in space weighted by the constant time step and temporally constant mesh volumes. Thus $\overline{\widetilde{U}}$ is effectively a space-averaging of corresponding time-averaged fine-mesh variables. It is usefully reminded that a time-averaged flow is much smoother than its instantaneous counterpart (Fig.4). Hence, no extra filtering is considered as necessary.

Similar to the time-averaging, when space-time averaging the original unsteady flow equations (Eq.1), we have $\overline{\widetilde{\boldsymbol{R}(\boldsymbol{U})}} = 0$, but $\boldsymbol{R}(\overline{\widetilde{\boldsymbol{U}}}) \neq 0$. Therefore, extra terms shall be needed to balance the flow equations with the space-time averaged flow variable $\overline{\widetilde{\boldsymbol{U}}}$, similar to the Reynolds-averaged flow equation in the direct mode (Eq.4).

Now, we may see how a direct mode and an inverse mode of the space-time averaged equations can be usefully made use of in the two domains respectively.

<u>*Space-Time Averaging* ('Direct Mode')</u>

The semi-discrete flow equations discretized on the global coarse-mesh domain can be expressed as

$$\frac{\partial \boldsymbol{U_C}}{\partial t} + \boldsymbol{R_C}(\boldsymbol{U_c}) = \boldsymbol{S_{st}} \tag{10}$$

Eq.10. means that a coarse-mesh domain solution can be driven towards a target by the space-time source term ($\mathbf{S_{st}}$) generated elsewhere (in the present work, it will be generated from the local fine-mesh solution as introduced in the following). Similar to Reynolds-averaging, when Eq.10 converges

to a steady state, the coarse mesh solution should produce a meaningful space-time averaged flow field, as long as proper source terms $\boldsymbol{S_{st}}$ can be provided.

Space-Time Averaging ('Inverse Mode')

$$\boldsymbol{S_{st}} = \boldsymbol{R_C}\left(\bar{\bar{\boldsymbol{U}}}_{\boldsymbol{f}}\right) \tag{11}$$

The input to Eq.11 will be based on the target space-time averaged fine-mesh solution $\bar{\bar{\boldsymbol{U}}}_{\boldsymbol{f}}$ to generate the source terms for the coarse-mesh discretization (thus 'R_C'). The source terms will drive the global coarse-mesh domain to a solution equivalently with a high resolution of the local fine-mesh domain. This is because the space-time averaged fine mesh solution $\bar{\bar{\boldsymbol{U}}}_{\boldsymbol{f}}$ will not hold in the under-resolved coarse-mesh equations due to the discretization errors. The coarse-mesh solution $\boldsymbol{U_C}$ will however be driven towards the target $\bar{\bar{\boldsymbol{U}}}_{\boldsymbol{f}}$, if the source $\boldsymbol{R}_C\left(\bar{\bar{\boldsymbol{U}}}_{\boldsymbol{f}}\right)$ is added to simply balance out the errors.

The combined applications of the 'direct mode' and the 'inverse mode' of the space-time averaging (Eqs.10 and 11) to the local fine-mesh and global coarse-mesh domains respectively underscore the inter-dependence between the two domains as the key ingredient of the approach:

a) If the source terms in Eq.10 (one scalar for each equation) can be provided to a global coarse-mesh domain, a converged coarse-mesh solution should then correspond to that as if the fine mesh be applied for the whole global domain.

b) If a global coarse-mesh is enabled to provide a right base flow environment, any truncated local fine-mesh domains within the global domain would then be able to produce a meaningful local solution of high resolution under right boundary conditions.

With the source terms linking the two domains through the direct and inverse modes of the space-time averaging respectively, we shall then be able to provide an effective closure for the under-resolved global coarse mesh domain, and to do so without resorting to an empirical turbulence model.

3. Two-Scale Solution Method

3.1. Dual Meshing and Interface Treatment

3.1.1. Global Coase-mesh and Local Fine-mesh

It is intended that the base mesh, though generally coarse, should be sufficiently fine so that large-scale disturbances in the outflow region are adequately captured and resolved. The fine-mesh domain is generated by embedding locally a fine-mesh block in the base coarse-mesh. An embedded fine mesh in a coarse base mesh in a near wall region is shown in Fig.5. For a compressor bladerow, the global base coarse mesh in multi-passage domain is shown in Fig.6a. The fine-mesh cells are generated by subdividing a coarse-mesh cell. In this case, only will one blade passage in a multi-passage domain need to be embedded with fine-mesh (around the bottom blade, Fig.6b).

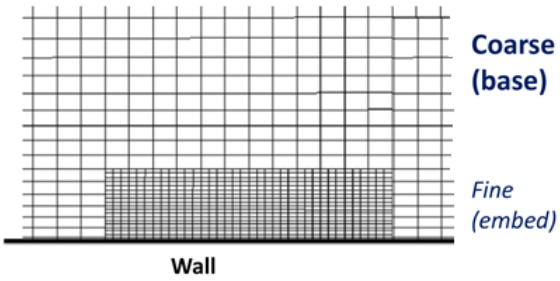

Figure 5: Local Fine-mesh block embedded in Global Coarse-mesh**.**

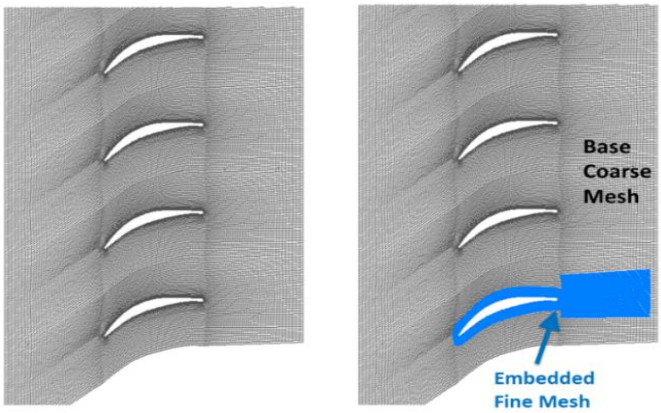

(a) Base Coarse-mesh (b) With Embedded Fine-mesh

Figure 6: Dual Meshes with Local Embedded Fine-mesh Blocks for Compressor Bladerow.

A point of note is that the dual mesh system also enables unsteady solutions in two different time steps while marching in time consistently. The large spatial length scale disparity also provides an opportunity for a time-marching with extra multi-stepping at a small time-step to enhance temporal resolution for the fine-mesh blocks locally. When time marching in a large time step for the coarse mesh region, we can take a number of fractional steps to time-march in the fine-mesh blocks. The boundary dummy points of the fine-mesh can then be interpolated from the corresponding coarse-mesh boundary points and between two large time instants.

3.1.2. Scale-Dependent Fine-Coarse Domain Interface Treatment

A main extra consideration is to do with the interface between the fine-mesh domain and the adjacent coarse-mesh one. Firstly the flux conservation for the interface boundary is enforced by overwriting the coarse-mesh boundary fluxes completely by the sum of the fluxes of the corresponding fine-mesh boundary faces.

The updating of an embedded block boundary needs to take into account the different mesh resolution between the two sides. It should be noted that nearwall flow has also been simulated previously with a local fine-mesh block called 'Minimum Flow Unit' (MFU), by Jimenez & Moin 1991 [16], Pascarelli et al 2000 [17], Tang & Akhavan 2016 [18], Sandham et al 2017 [19] and Carney et al 2020 [20]. The common limit of all those previous MFU setups however is the direct periodicity imposed in the two wall parallel directions. The direct periodicity would clearly impede the outer flow large scale 'foot-

printing' on the near wall flow, unless the MFU is taken to be very large (thus with little/no computational-cost benefit). To enable the local near-wall fine-mesh block to 'see' outer flow large scales, a scale-dependent interface treatment (He, 2018 [2]) is adopted. A flow variable at the fine-mesh block boundary is split into two parts, a base coarse-mesh resolved component and a fluctuation corresponding to the fine-mesh resolution:

$$\boldsymbol{U}(\boldsymbol{x},\boldsymbol{t}) = \quad \boldsymbol{U_C}(\boldsymbol{x},\boldsymbol{t}) \quad + \quad \boldsymbol{\Delta U'_f}(\boldsymbol{x},\boldsymbol{t}) \tag{12}$$

$\boldsymbol{U_C}$ is the base coarse-mesh resolved part, directly interpolated from the surrounding coarse-mesh points. The small-scale fluctuating disturbance $\boldsymbol{\Delta U'_f}$, subject to the fine-mesh resolution, can then be taken from a corresponding mesh point from its pairing counterpart boundary. The treatment of the fine-mesh fluctuation part is similar to an inflow turbulence generation at an upstream boundary by recycling the unsteadiness from a downstream boundary counterpart. For instance, given an inflow from the left to the base-mesh domain as shown in Fig.1a, '***z1'*** is a boundary mesh point on a side boundary of the fine-mesh block with its counterpart pairing mesh point *'***z2'*** on the other side of the fine-mesh block. The recycling condition is then only applied to the fine-mesh fluctuation part:

$$\boldsymbol{\Delta U'_f}(\boldsymbol{x},\boldsymbol{t})_{\boldsymbol{z1}} = \boldsymbol{\Delta U'_f}(\boldsymbol{x},\boldsymbol{t})_{\boldsymbol{z2}} \tag{13}$$

For a stator-rotor interface, the embedded fine-mesh in the upstream bladerow also provides a useful means of generating fine-mesh resolved turbulence fluctuating inflow disturbances for all passages of the downstream bladerow. The instantaneous spatial distribution of unsteady disturbances of the fine mesh passage is firstly obtained by a circumferential Fourier spectrum at the interface (He 2021 [33]). This spatial spectral distribution should contain high harmonics representing the small scales resolved in the wake region of the upstream fine-mesh passage. In constructing the instantaneous inflow disturbance characteristics for the downstream bladerow, the low harmonics are taken locally from the coarse-mesh passages respectively. The high harmonics of the upstream fine-mesh passage should be used with corresponding phase-shift to align with the local wakes of the coarse-mesh passages. Thus, all passages of the downstream blade row can be effectively subject to instantaneous inflow-wake fluctuating disturbances of the fine-mesh resolution of the upstream single-passage.

3.2. Global-Local Domain Interaction

The solution procedure is aimed to leverage the interaction between the global coarse-mesh and the local fine-mesh. During the solution process, each of the two parts has its own 'intermedium' target:

a) the target resolution from the local fine-mesh domain to correct the global coarse-mesh.

b) the target conditioning from the global coarse-mesh to correct the local-mesh domain.

When this coupled procedure converges with no further corrections needed, we shall then have the desired solutions for both parts: much improved resolution for the otherwise under-resolved coarse-mesh domain, and much improved conditioning for the otherwise poorly-conditioned local fine-mesh domain. The following are some key aspects of the solution procedure.

3.2.1. Generation of Source Terms

The target for the coarse-mesh domain is the fine-mesh solution when temporally and spatially averaged on the corresponding coarse-mesh cells. In addition, as discussed earlier, we should only propagate time-averaged parameters. Hence, we generate source terms from the space-time averaged flow solution in the local fine-mesh domain.

Firstly, we need to perform the time-averaging during the time-marching solution. This is carried out in a moving-average (e.g. He, 2018 [2]). This is a very straightforward updating operation and we only need to store the space-time averaged in the coarse-mesh cells for one time-step. Having updated the equivalent target coarse-mesh solution ($\overline{\widetilde{U}}_f$), we then simply use the inverse mode (Eq.11) of the space-time averaging to explicitly and non-iteratively obtain the scalar source terms.

The source terms for the global coarse-mesh can be generated in two different sequences between the source-term generation and propagation. The baseline method is to first generate source terms locally in the fine-mesh domain using the space-time averaged flow variables before propagating the generated source terms to the global domain. This is labelled as a '***generation-propagation***' source term procedure. The second option is to first propagate the space-time averaged flow variables from the fine-mesh solution to the global coarse-mesh before working out the source-terms locally in the global domain (He 2023 [21]). This is labelled as a '***propagation-generation***' source-term procedure. For a simple uniform structured mesh, the two sequences are equivalent to each other. For more complex meshes with nonuniform (structured or unstructured) meshes, the dependence of the source-terms on mesh size and geometry means that the second option would effectively be an in-situ 'mesh-informed' source term generation procedure. When the coarse-mesh solution becomes unsteady, there is an additional source term due to the time-averaging on the coarse mesh. The details of the time-averaging term can be found in He 2018 [2].

At this point, a different but relevant context should be noted. There are some on-going efforts on developing machine-learned wall-function condition for coarse-mesh LES without a near-wall RANS model (e.g. [22-26]). A closely relevant issue for such wall-function models is that the accuracy and effectiveness of these models may be considerably mesh-dependent, as discretization errors will inevitably be nonnegligible when a under-resolved coarse-mesh is used as meant to be for WMLES. It can be argued that a generalizable learned wall-condition model will have to be 'mesh-informed'.

3.2.2. Propagation of Fine-mesh Resolution Effect to Global Coarse-Mesh

Now we consider the propagation of the high-resolution results gathered from the local fine-mesh blocks to the global coarse-mesh. Firstly, note that the space-time averaged flow field tends to be smooth, much smoother than the instantaneous one. Thus, a spatial variation of the space-time averaged variables (either the source terms or the fine-mesh solution) is amenable to a spectral representation.

A mesh-pointwise variation among the fine-mesh blocks can be accurately represented by a block-to-block spectrum for the corresponding mesh point in all fine-mesh blocks, which is thus called 'Block Spectrum'. Furthermore, for a near wall region, a block spectral propagation will only need to be

carried out in the two wall parallel directions. The detailed formulations for a block-spectral mapping based on a double Fourier series can be found in He (2013[1], 2018[2]).

It is worth mentioning that the baseline Fourier series is for a periodic distribution. For a nonperiodic distribution, a half-range Fourier series can be used, as He 2013[1]). Chebyshev spectral method is a common choice, as also implemented in Chen and He 2023 [3]. It is found with a detailed derivation that the two (the half-range Fourier and Chebyshev spectra) are actually the same (He, 2023 [27]). Noted also is that the local-to-global domain mapping is also implementable with a Machine-Learning method, as shown by Yao & Chen 2024 [28].

Fig.7 is the solution flow chart, indicating the main parts and actions of the coupling between the two domains reflecting the corresponding two-scale interaction.

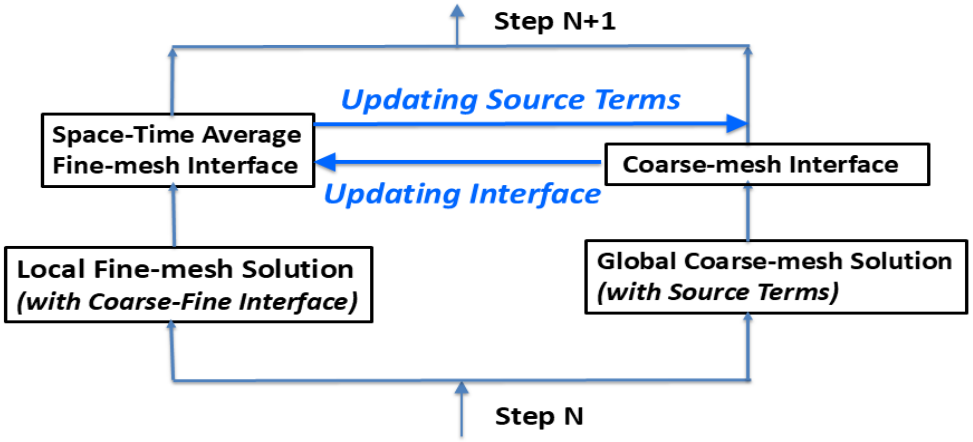

Figure 7: Flow-chart for Two-scale Coupling in One Solution Step.

3.3 Balanced Eddy Viscosity (BEV) for Robust Coarse-mesh Solution

It is recognized that the solutions to flow equations with added Reynolds stresses may experience convergence issues. As discussed for source term driven solutions (He 2018 [2] for, 2023 [21], Zhang and He 2018 [30]), the eddy viscosity in commonly adopted in turbulence models can enhance convergence robustness of the source terms driven solutions. Wu et al, 2019 [29] attributed an improved conditioning to an implicit (instead of explicit) implementation of Reynolds stresses. It is argued however that the real cause for the improvement might well arise from the eddy viscosity used in the implementation process rather than the implicit scheme itself (He 2023 [21]).

In the context of the two-scale method, a key requirement is that any numerical damping in the coarse-mesh solution process should have no effect on the final time-averaged solution when approaching the space-time averaged target. The Balanced Eddy Viscosity (BEV) (He, 2018 [2]) is adopted, implemented in form of a sub-grid scale (SGS) model for LES, to limit its influence on the coarse-mesh resolved large scale unsteadiness (He 2023 [21]).

Consider a simple eddy-viscosity model based on the target time-averaged flow propagated from the fine mesh.

$$\mu_T = \widetilde{\overline{\rho}_f} l^2 \left|\widetilde{\overline{\Omega}_f}\right| \quad (14)$$

The mixing-length is capped by a maximum length L_m :

$$l = ky \quad (y < l_m) \quad (15a)$$

$$l = l_m \quad (y > l_m) \quad (15b)$$

where k is the von Karman constant, 0.41; y is the distance to the wall and l_m is a maximum mixing length. A limit length is taken relative to the local mesh-size similarly to a sub-grid scale model.

$$l_m = \min(ky, C_{ev} l_{SGS}) \quad (16)$$

l_{SGS} is the local length scale for a sub-grid scale model. For the Smagorinsky model, $l_{SGS} = C_{SGS}\Delta_{mesh}$ ($a\ nominal\ value, C_{SGS} = 0.16$). Δ_{mesh} is the local mesh size, C_{ev} is the coefficient to control the eddy-viscosity damping.

Note that the eddy viscosity is worked out based on the space-time averaged flow variables (Eq.14). Thus, the corresponding viscous stresses added to the momentum equations are linear, so are the corresponding heat conduction terms in the energy equation. We can lump all these linear terms together denoted as vector L. Take the difference between the lump linear terms updated with the coarse-mesh solution and those based on the target solution: $L(\boldsymbol{U_C}) - L(\widetilde{\overline{\boldsymbol{U}}}_{\boldsymbol{f}})$. Add this difference to the coarse-mesh equation (Eq.10). The two terms will be balanced out with zero net effect when the time-averaged solution $\overline{\boldsymbol{U}}_C$ on the coarse-mesh approaches the target solution $\widetilde{\overline{\boldsymbol{U}}}_f$, (He 2023 [21]).

4. Some Examples

The two-scale framework methodology has been implemented, validated and demonstrated in several CFD codes for compressible flow RANS/URANS and LES solutions ([1], [2], [31-34]) and incompressible flow LES solutions ([3],[35]). Here we will look very briefly at some sample LES results. More details and discussions on these and other cases can be found the related references.

4.1. Channel Flow

Given the range of potential applications, the two-scale method should be validated in some general and fundamental settings. It has been implemented in an incompressible flow open-source solver (OpenFOAM). The method is first examined at a canonical channel flow (Chen and He 2022 [3]).

4.1.1. Sizing Nearwall Fine-mesh Block

The choice of the embedded fine-mesh block size should meet the target requirements for the solution in the nearwall region: to both resolve the 'universal' part of the near-wall turbulence and capture the 'foot-printing' effects of large coherent structures of the outer flow.

The selection of the near-wall fine-mesh block size is based on examining DNS data for an incompressible channel flow (Lee & Moser 2015) [11]. Based on the desired attribute for the embedded block to capture and resolve the 'universal' turbulence behavior, the block sizes are taken to be constant in wall units in the streamwise and spanwise directions respectively, $l_x^+ \approx 3500$ and $l_z^+ \approx 350$ (Chen

and He 2022 [3]). These block dimensions are in line with those taken previously for minimum flow unit (MFU), e.g. Carney et al 2020 [20]. In the wall-normal direction, the fine-mesh block needs to resolve both the small scales in the inner near wall region and capture the influence of the large scales resident in the log-law region. Thus, the wall normal size of the local fine-mesh block is taken to cover the starting location of the log-law region correlated directly to friction Reynolds number (Marusic, et al 2013 [36]), $l_y^+ \approx 3\sqrt{Re_\tau}$.

4.1.2. 'Foot-printing' of Outer Flow on Inner Near-wall Flow

The raw data of instantaneous streamwise velocity disturbances on the cut planes at an inner location (y^+=13.5) and outer log-law region (y^+=175) are shown in Fig.8. The results clearly indicate the 'foot-printing' of the outer large scales on the inner region, unimpeded by the local fine-mesh block.

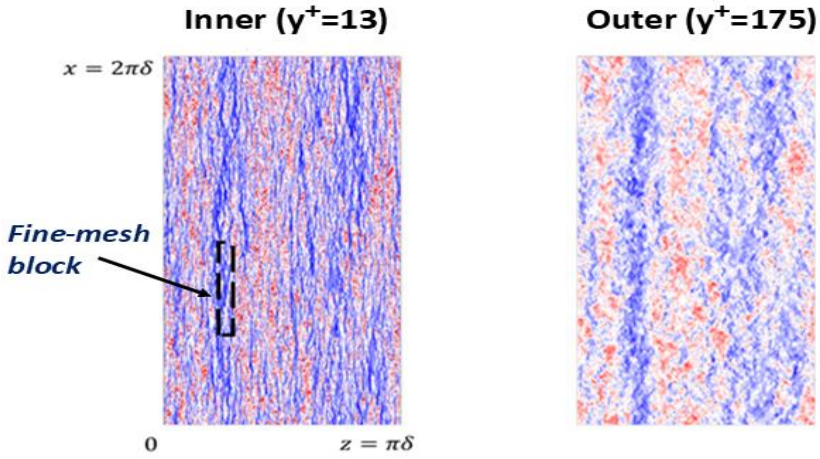

Figure 8: Instantaneous Velocity Disturbances on Inner (y^+=13) and Outer (y^+=175) Cut-planes [3]

4.1.3. Scale Separation/'Spectral Gap'?

A key aim of the present development in relation to WMLES is to avoid spectral-gap/'scale-separation'. The length scale range captured by the fine-mesh solution of the local embedded fine-mesh block is given in terms of the frequency power spectral density (PSD) as shown in Fig. 9, for a channel flow at $Re_\tau \approx 1000$. The data are obtained at two locations of the same wall normal distance $y^+ = 13.5$: at the middle of the embedded fine-mesh block and at a coarse-mesh point outside the embedded block.

It can be seen clearly that the spectrum from the local fine-mesh block indicates a full spectra range. On the other hand, the global coarse-mesh region is clearly subject to an under-prediction for the small-scale high frequency part as expected. Thus, although the present method is phenomenologically based on a two-scale framework, there is no scale-separation assumed, nor is any scale-separation/spectral gap observed.

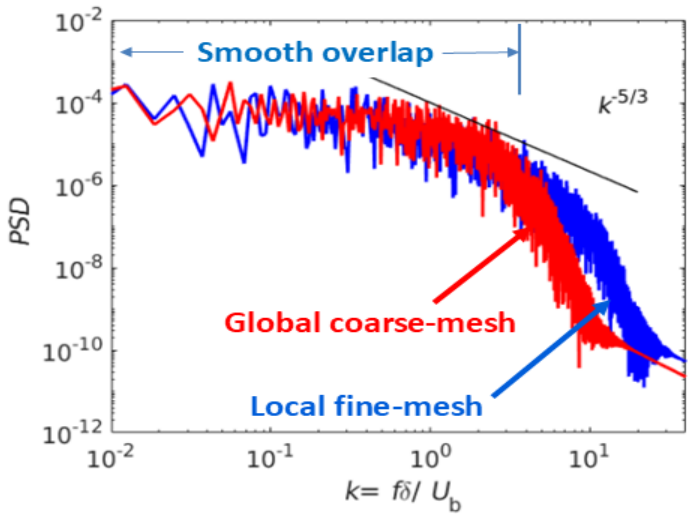

Figure 9: Turbulence power spectra density (PSD) as function of non-dimensional frequency [3]

4.1.4. Validation against DNS for Different Reynolds Number

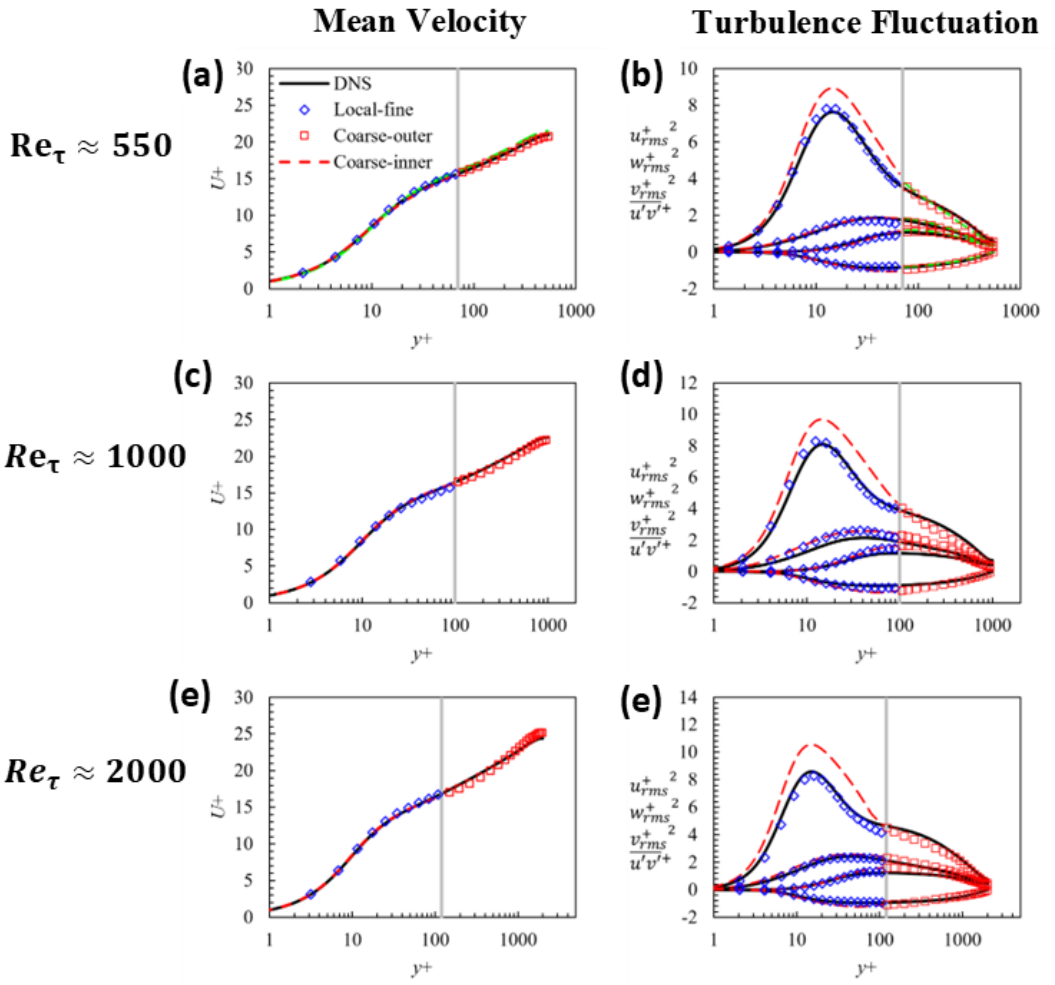

Figure 10: Mean velocity (a, c, e) and turbulence fluctuation (b, d, f) [3], compared with DNS [11].

4.2. Tripped Turbulent Boundary Layer (Chen and He 2023 [35])

4.2.1. Valdiation against DNS and WRLES

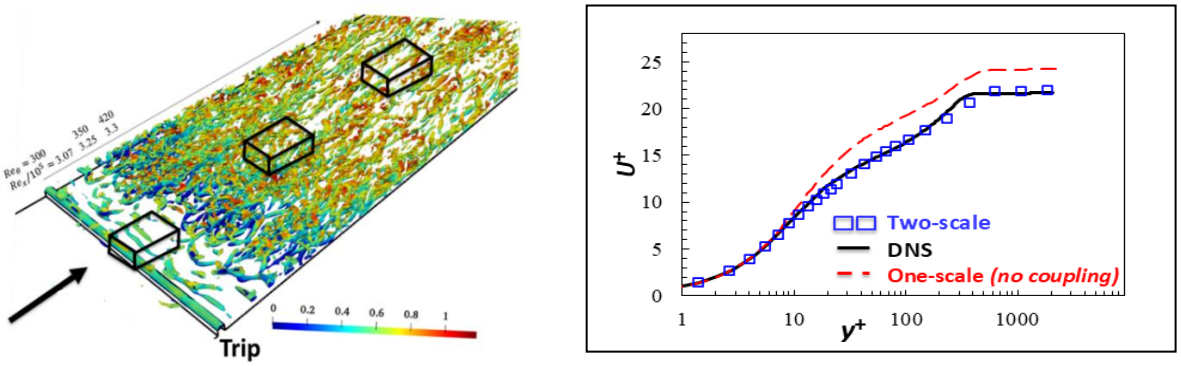

Figure 11: Tripped Turbulent Boundary Layer: mean velocities in coarse-mesh region at $Re_\theta \approx 1000$. Two-scale solution [35] are compared with the DNS data [37]. Also included is the 'one-scale' solution (without the source-term coupling).

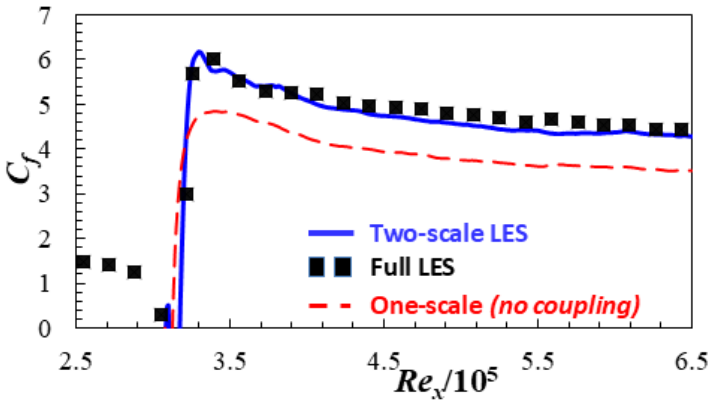

Figure 12: Friction coefficient C_f as function of Reynolds number Re_x [35]

4.2.2. Mesh-count Scaling with Reynolds Number

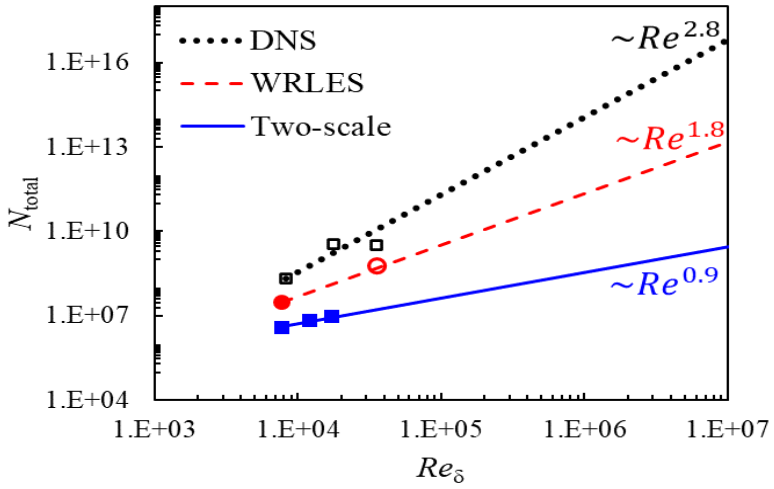

Figure 13: Mesh count - Re scaling [35]

4.3. Turbomachinery Configurations

The following test cases are examined to assess the two-scale method implemented in an in-house compressible flow solver. A more tangible objective is to see if a local single-passage fine-mesh can be effectively embedded in a multi-passage coarse-mesh domain with a fine/coarse mesh density ratio ~O(10^2). More detailed descriptions and discussions can be found in He 2021 [33].

4.3.1. Compressor Cascade with Flow Separation Induced Transition

The scale-resolving capability is consistently indicated by the iso-surface plots of the Q criterion (Fig.14). Also included are surface pressures compared with the experiment [38].

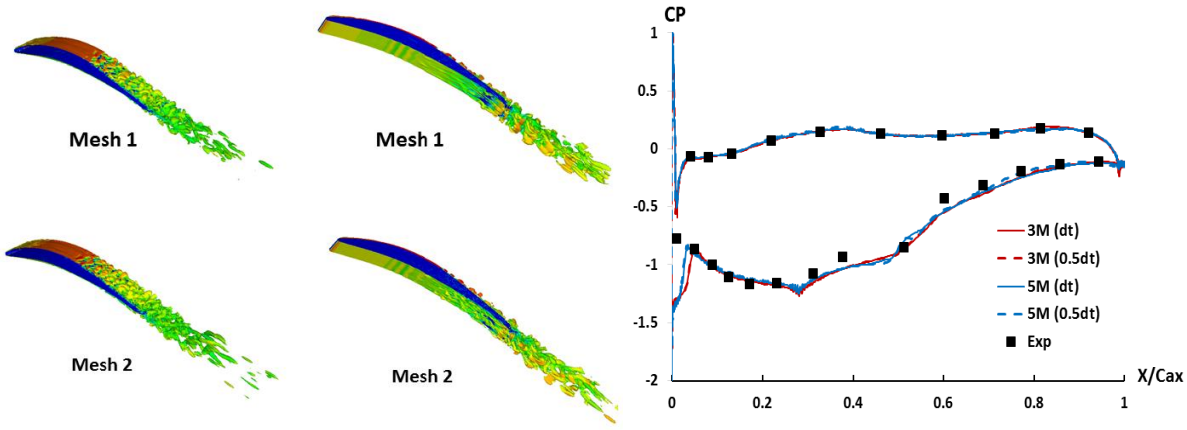

a) Suction Surface View b) Pressure Surface View c) Surface Pressures

Figure 14: Numerical Sensitivity (10% span sector) [33]

A mid-chord separation on the suction surface is shown at around 40% chord with a subsequent transition to turbulent flow, in agreement with the experimental observation [38]. Also there appears to be a transitional behavior on the pressure surface (Fig.14b). Overall, the mesh resolution of Mesh 1 (3 million mesh cells for a 10% span sector) seems able to provide sufficient scale-resolving capability.

We then examine the two-scale method for multiple blade-passages under an inlet distortion (Fig.15, Fig.16). The global multi-passage domain is on a RANS-like coarse-mesh. The fine-mesh is used only for the bottom passage. The mesh density ratio (embedded fine-mesh/base coarse-mesh) is 72.

The unsteady distorted flow pattern in terms of an entropy function is shown in Fig.15. Also presented in Fig.15 is the downstream traverse comparison of time-averaged axial velocities. Three solutions are compared: the direction solution with the fine-mesh for all 6 passages, the two-scale solution with only a single-passage fine-mesh coupling with the other 5 passages on the base coarse-mesh, and a URANS solution on the base mesh.

The comparisons in unsteady vorticity and time-averaged velocities are given in Fig.16. Note specifically the differences between the two-scale and the URANS solutions (Figs.16b, 16c). Both have the same coarse-mesh for the upper 5 blade passages in the domain. We can see the dissipative 'damping' effect of the eddy viscosity in URANS on the trailing edge vortex shedding and unsteady wakes. The good agreement in time-averaged results between the direct multi-passage fine-mesh solution and the two-scale solution is clearly and consistently demonstrated in both the downstream traverse (Fig.15) and the velocity field (Figs.16d,16e), as the primary objective of the approach.

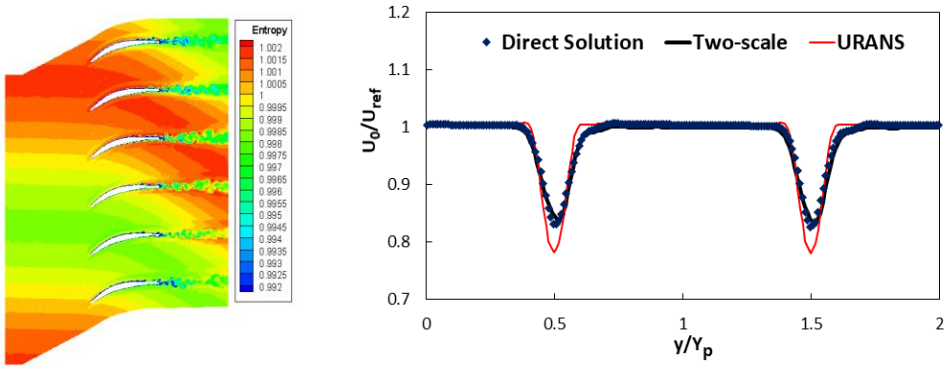

Figure 15: Compressor Cascade with Inlet Distortion (overall pattern and exit velocity traverse [33])

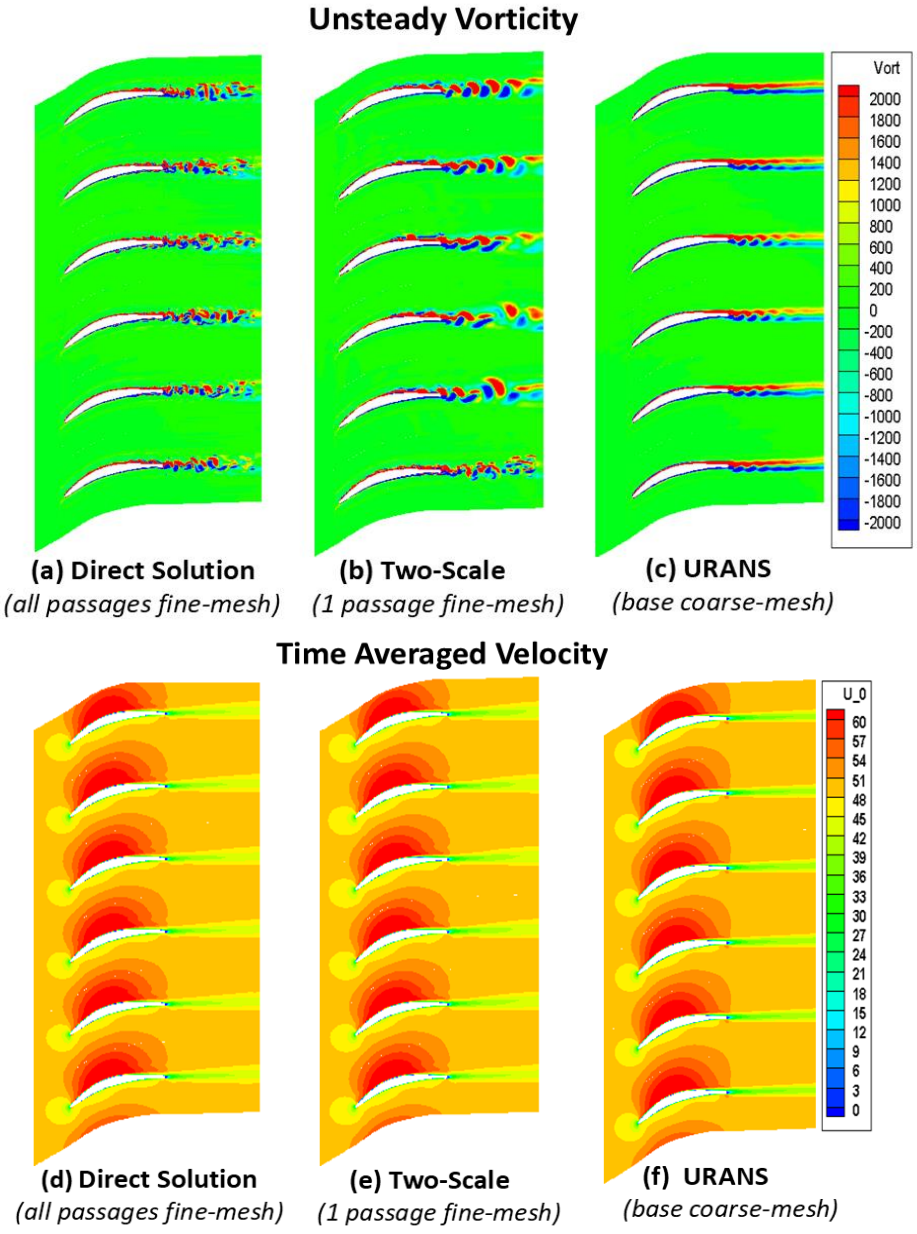

Figure 16: Compressor Cascade with Inflow Distortion, Unsteady (top) vs Time-average (bottom) [33].

4.2.2. Transonic Turbine Stage

To assess the multi-passage multi-bladerow capability, a high-pressure transonic turbine stage is examined. Figure 17 shows the base coarse-mesh and the fine-mesh embedded in a single passage for each blade row respectively. Figure 18 compares the instantaneous (top) and time-averaged entropy contours (bottom) between the direct solution, the two-scale solution and a full turbulent URANS solution. The agreement in the time-averaged results between the direct fine-mesh solution and the two-scale single-passage fine-mesh solution underline the validity of the two-scale method. In this case, the embedded fine/coarse mesh density ratio is 160.

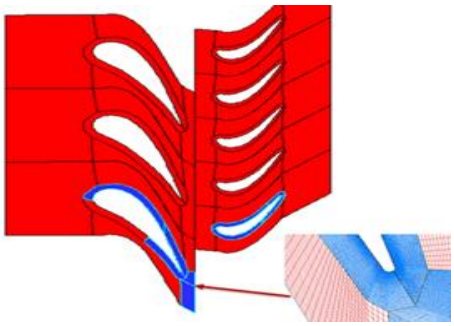

Figure 17: Turbine Stage Domain with Embedded Fine Mesh in Single Passage for Each Row [33].

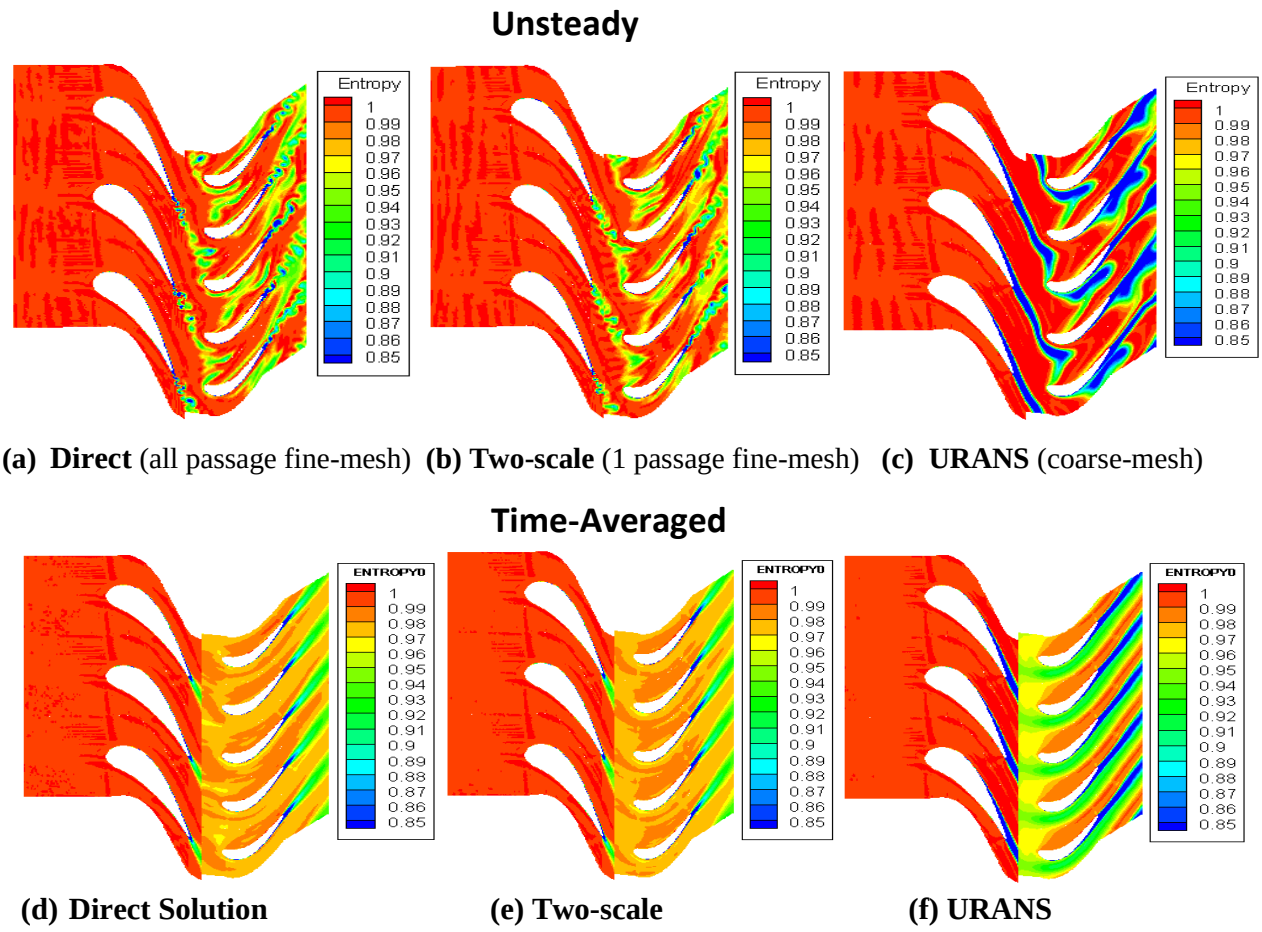

Figure 18: Unsteady (top) and Time-average (bottom) Entropy Function ($e^{(-\Delta S/R)}$) [33].

Finally, a stage configuration with 10 stator and 19 rotor passages is taken to illustrate potential impact of the two-scale method for larger multi-passage/whole annuls domains of more realistic blade counts. The fine-mesh blocks are embedded in the base coarse-mesh in the near-wall and wake regions of a single-passage for each row. The corresponding fine/coarse mesh density ratio is 128. For this case a direct multi-passage fine-mesh would be very time-consuming. The two-scale solution with fine mesh blocks embedded only in a single-passage per row is a much more efficient and affordable alternative.

The instantaneous and time-averaged entropy contours for the overall domain configuration are shown in Fig.19. The differences in mesh resolution between the base coarse-mesh and the embedded fine mesh are clearly identifiable in the unsteady entropy contours. On the other hand, the time-averaged flow of those coarse-mesh passages agrees well that of the single passage embedded with the fine-mesh (the bottom passage of each row), underlining the impact of the source-term coupling, which is at the heart of the two-scale framework.

It should be reminded that the primary means of validating the two-scale single passage fine-mesh solution is to compare it with a direct multi-passage fine-mesh solution. As such the blade counts taken (thus the number of blades of the domain) need to be small enough to be able to run the direct solutions in a reasonable time-frame (e.g. the case shown in Figs.17, 18). For a realistic blade count, there will have to be significantly larger numbers of passages (e.g. as indicated in the case shown in Fig.19). The cost of a direct solution will have to scale with the number of blade passages accordingly. However, the cost of the two-scale solution with only a single passage fine-mesh per row should be largely the same, regardless of the blade counts. Therefore, we can see that the two-scale method should have considerable potential for a turbulence scale-resolving solution of an equivalent high fidelity, but at a fractional cost of a conventional direct multi-passage/whole annulus fine-mesh solution.

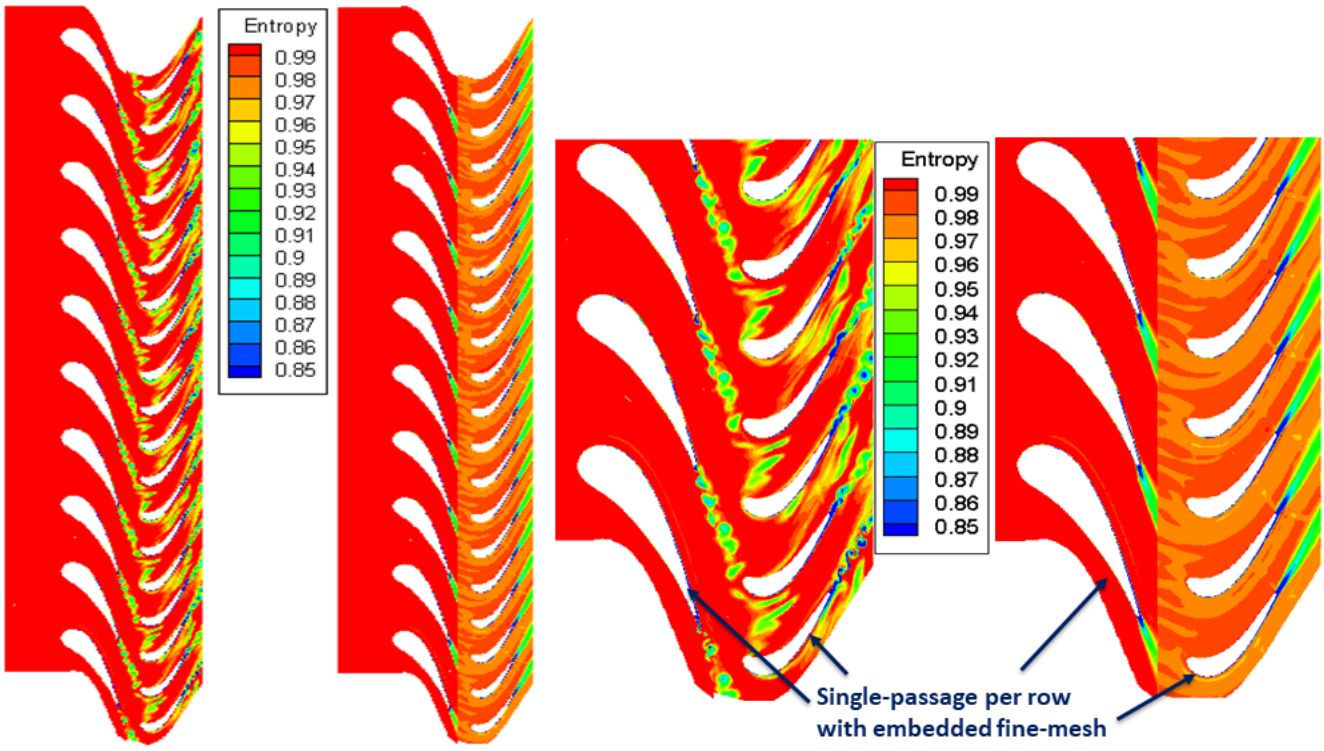

Figure 19: Contours of Entropy Function, $e^{(-\Delta S/R)}$ (Stator/Rotor Count: 10/19) [33].

Closing Remarks

In the context of scale-resolving methods for wall-bounded turbulent flows, the two-scale LES is aimed to be much more computationally efficient than WRLES and to be much less empirical than WMLES. Like WMLES, the computational cost benefit is achieved by using a coarse-mesh in the near wall region. We then have to face the issue of under-resolution caused errors both in the near-wall interior domain and on the wall boundary. A coarse-mesh LES solution for near-wall region is therefore inherently mesh-dependent. As such, an effective correction on the under-resolution associated errors will need to be 'mesh-informed'. A further motivating consideration arises from the recent findings on the Re-dependent inner near-wall flow behavior due to outer flow large-scale influence and scale-interaction.

Given the context, we introduce locally embedded fine-mesh block(s) in order to

a) capture large scale influence from outer flow region, and resolve small scales and dominant inner-outer interaction in the local fine-mesh near-wall region.

b) generate and propagate 'mesh-informed' source-terms to correct (balance out) the under-resolution associated numerical errors in the global coarse-mesh in near-wall region.

A space-time averaging is adopted to link a fine-mesh and its coarse-mesh counterpart. By casting the space-time averaging in an 'inverse-mode', we use the local fine-mesh solution to generate the source terms for the global coarse-mesh domain while advancing the fine-mesh solution conditioned by the global domian. At the same time, by casting the space-time averaging in a 'direct-mode', we advance the global coarse-mesh solution driven by the source terms arising from the local fine-mesh solution. A converged solution of the coupled two-scale system should meet two seemingly conflicting requirements: an otherwise poorly conditioned local fine-mesh domain will now be subject to a more adequate environment and flow condition, and an otherwise poorly resolved global coarse-mesh domain will now be effectively subject to a high resolution.

The framework methodology has been implemented in incompressible and compressible flow solvers, validated at canonical settings, against well-established DNS and full LES results. Potential computational cost benefit manifests in terms of much reduced mesh count-Reynolds number scaling: from ~O(Re^2) for full WRLES to ~O(Re) for the two-scale LES. The two-scale method has also been tested for realistic turbomachinery flow configurations with embedded fine-mesh/base coarse-mesh density ratios ~O(10^2).

References

1. He, L., 2013 "Block-Spectral Mapping for Multi-Scale Solution", Journal of Computational Physics, Vol.250, pp13-26.

2. He, L., 2018 "Multiscale Block Spectral Solution for Unsteady Flows", International Journal for Numerical Methods in Fluids, Vol.86, Issue 10.

3. Chen, C., and He, L, 2022 "On Locally Embedded Two-scale Solution for Wall-bounded Turbulent Flows", Journal of Fluid Mechanics, Vol.933, A47.

4. Jimenez, J., 2003 "Computing high-Reynolds-number turbulence: will simulations ever replace experiments?" Journal of Turbulence, **4**, pp. 1-14.

5. Mizuno, Y. & Jiménez, J., 2013 "Wall turbulence without walls". Journal of Fluid Mechanics, **723**, pp. 429-455.

6. Spalart, P. R., Jou, W.-H., Strelets, M. & Allmaras, S., 1997 "Comments on the feasibility of LES for wings, and on a Hybrid RANS/LES approach". Ruston, Louisiana, USA, Proceedings of the First AFOSR International Conference on DNS/LES.

7. Spalart, P. R., 2009. "Detached-Eddy Simulation." Annual Review of Fluid Mechanics, **41**, pp. 181-202.

8. Hutchins, N. & Marusic, I., 2007, "Evidence of very long meandering features in the logarithmic region of turbulent boundary layers." Journal of Fluid Mechanics, **579**, pp. 1-28.

9. Marusic, I., Mathis, R. & Hutchins, N., 2010, "Predictive Model for Wall-Bounded Turbulent Flow." Science, **329**(5988), pp. 193-196

10. Jimenez, J., 2013. "Near-wall turbulence". Physics of Fluids, **25**(10), p. 101302.

11. Lee, M. & Moser, R., 2015. "Direct numerical simulation of turbulent channel flow up to $Re_\tau \sim 5200$". Journal of Fluid Mechanics, **774**, pp. 395-415.

12. Mathis, R., Hutchins, N. & Marusic, I., 2009. "Large-scale amplitude modulation of the small-scale structures in turbulent boundary layers." Journal of Fluid Mechanics, **628**, pp. 311-337.

13. Agostini, L. & Leschziner, M. A., 2016, "Predicting the response of small-scale near-wall turbulence to large-scale outer motions." Physics of Fluids, **28**(1), p. 015107.

14. Denton, J.D., 1986, "The Use of a Distributed Body Force to Simulate Viscous Flow in 3D Flow Calculations," ASME Paper 86-GT-144.

15. Ning, W. & He, L., 2001 "Some modeling issues on trailing-edge vortex shedding". AIAA Journal, Vol.39(5), pp. 787-793.

16. Jimenez, J. & Moin, P, 1991 "The minimal flow unit in near-wall turbulence". Journal of Fluid Mechanics, **225**, pp.213-240.

17. Pascarelli, A., Piomelli, U. & Candler, G., 2000. "Multi-Block large-eddy simulations of turbulent boundary layers." Journal of Computational Physics, **157**(1), pp. 256-279.

18. Tang, Y. & Akhavan, R., 2016. "Computations of equilibrium and non-equilibrium turbulent channel flows using a nested-LES approach." Journal of Fluid Mechanics, **793**, pp. 709-748.

19. Sandham, N., Johnstone, R. & Jacobs, C., 2017. "Surface-sampled simulations of turbulent flow at high Reynolds number." International Journal for Numerical Methods in Fluids, **85**(9), pp.525-537

20. Carney, S., Engquist, B. & Moser, R., 2020. "Near-wall patch representation of wall-bounded turbulence." Journal of Fluid Mechanics, **903**, p. A23.

21. He, L., 2023, "Two-scale Conjugate Heat Transfer Solution for Micro-structured Surface", International Journal for Numerical Methods in Fluids, Vol.95, Issue 8, pp.1260-1285.

22. Bae, H.J., and Koumoutsakos, P. 2022, "Scientific multi-agent reinforcement learning for wall-models of turbulent flows". Nat. Commun. **13** (1), 1–9.

23. Lozano-Durán, A., and Bae H. J., 2023 "Machine learning building-block-flow wall model for large-eddy simulation", Journal Fluid Mechanics, Vol.963, A35.

24. Maejima, S., Tanino, K., and Kawai, S., 2024, "Physics-informed machine-learning solution to log-layer mismatch in wall-modeled large-eddy simulation", Physical Review Fluids, Vol.9, 084609.

25. Zhou, D., and Bae H. J., 2024, "Wall modeling of turbulent flows with various pressure gradients using multi-agent reinforcement learning." AIAA Journal, Vol.62, No.10.

26. Davidson, L., 2025 "Hybrid LES/RANS for flows including separation: a new wall function using machine learning based on binary search trees", Journal of Turbulence, Vol.26, Issue 2-3.

27. He, L. 2023 "Spectral Heat Transfer Coefficient for Convection", International Journal of Heat and Mass Transfer, Vol.216, 124557.

28. Yao, M. and Chen, C. 2024, "On Machine-Learning-Aided Two-Scale Solution for Turbulent Fluid Flows", AIAA Journal, Vol.62, No.4.

29. Wu, J, Xiao H., Sun, R. and Wang, Q., 2019. "Reynolds-averaged Navier–Stokes Equations with Explicit Data-driven Reynolds Stress Closure can be Ill-conditioned". Journal Fluid Mechanics, 869, pp553-586.

30. Zhang, M., and He, L., 2018 "An Efficient Large Eddy Simulation Method for Blade Trailing Edge Cooling Optimization", AIAA Journal of Propulsion and Power, Vol. 34, No.4.

31. He, L, and Yi, J., 2017, "Two-Scale Methodology for URANS / Large Eddy Simulation Solutions of Unsteady Turbomachinery Flows", Journal of Turbomachinery, Vol.139, Issue 10.

32. Duan, P.H. and He, L, 2020 "Application of Multi-scale Methodology for Transonic Turbine Blade Tip Cooling Design", Journal of Turbomachinery, Vol.142, Issue 8.

33. He, L., 2021 "Averaging for High Fidelity Modeling - Toward Large Eddy Simulations in Multi-Passage Multi-Row Configurations", Journal of Turbomachinery, Vol.143(2): 021002.

34. Phan, H.M., and He, L, 2021 "Efficient Steady and Unsteady Flow Modeling for Arbitrarily Mis-Staggered Bladerow under Influence of Inlet Distortion", J. Eng. Gas Turbines Power**,** Vol.143(7), 071009.

35. Chen, C., and He, L., 2023. "Two-scale Solution for Tripped Turbulent Boundary Layer." Journal of Fluid Mechanics, Vol.955, A5.

36. Marusic, I., Monty, J., Hultmark, M. & Smits, A., 2013. "On the logarithmic region in wall turbulence." Journal of Fluid Mechanics, Vol.716, R3.

37. Schlatter, P. & Orlu, R., 2012. "Turbulent boundary layers at moderate Reynolds numbers: inflow length and tripping effects". Journal of Fluid Mechanics, Vol.710, No.1.

38. Yang H., and He, L. 2004. "Experimental Investigation of Linear Compressor Cascade with 3-D Blade Oscillation". AIAA Journal of Propulsion and Power, Vol.20, No.1.